Applied Physics Letters

Thermal budget increased alloy disorder scattering of 2DEG in III–N heterostructures

Cite as: Appl. Phys. Lett. **120**, 213504 (2022); https://doi.org/10.1063/5.0093839
Submitted: 30 March 2022 • Accepted: 16 May 2022 • Published Online: 26 May 2022

Hao Yu, Bertrand Parvais, Ming Zhao, et al.

Applied Physics Letters ARTICLE scitation.org/journal/apl

Thermal budget increased alloy disorder scattering of 2DEG in III–N heterostructures

Cite as: Appl. Phys. Lett. **120**, 213504 (2022); doi: 10.1063/5.0093839
Submitted: 30 March 2022 · Accepted: 16 May 2022 ·
Published Online: 26 May 2022

Hao Yu,[1,a)] Bertrand Parvais,[1,2] Ming Zhao,[1] Raul Rodriguez,[1] Uthayasankaran Peralagu,[1] Alireza Alian,[1] and Nadine Collaert[1]

AFFILIATIONS

[1]imec, Kapeldreef 75, Heverlee 3001, Belgium
[2]Department ETRO, Vrije Universiteit Brussel, Brussel 1050, Belgium

[a)]Author to whom correspondence should be addressed: hao.yu@imec.be

ABSTRACT

High-temperature processing steps are frequently used in manufacture of AlGaN/(AlN/)GaN high electron mobility transistors (HEMTs). The thermal budgets drive Al diffusion into the GaN channel, increase alloy disorder scattering (ADS) of the two-dimensional-electron-gas (2DEG), and degrade the 2DEG mobility. By correlating the ADS to device thermal budget, we propose an analytical model to calculate the ADS limited mobility as a function of Al diffusion lengths ($L_{D,Al}$) in AlGaN/(AlN/)GaN HEMTs. The simulation indicates that the ADS is a significant mobility degradation mechanism whose scattering rate increases with the 2DEG density and the $L_{D,Al}$. The findings explain the generally observed trends in the literature that the 2DEG mobility and sheet resistances of GaN heterostructures degrade with increased thermal budgets, especially after >900 °C processing.

GaN high electron mobility transistors (HEMTs) are attractive for power electronics and radio frequency applications.[1–4] In the past two decades, advanced III–N epitaxy techniques have boosted maturity of GaN HEMT technology. High temperatures of 600–1200 °C are required to epitaxially grow high-quality III–N layers because of high formation energy of III–N bonds.[5] Molecular beam epitaxy of III–N (MBE) is performed at relatively a low temperature below 850 °C but has a low growth rate; metal-organic chemical vapor deposition (MOCVD) of III–N featuring a fast growth rate and a large production scale is, however, performed at a wide temperature range of 700–1200 °C [see benchmarks in Fig. 4(c) for examples]. Due to high-temperature growth, a barrier and sometimes a thin AlN interlayer (IL) in GaN HEMTs make a high post-GaN channel thermal budget. Moreover, III–N surface passivation, source/drain formation, gate formation, and back-end-of-line (BEOL) processing also add to thermal budgets. In this work, we elaborate on a major adverse effect of the post-channel thermal budgets—increased alloy disorder scattering (ADS) of the two-dimensional-electron-gas (2DEG) in a GaN channel.

In recent literature, there has been increased focus on correlating the thermal budget of GaN heterostructures with electrical properties of the 2DEG. On the one side, it is noted that a high post-channel thermal budget leads to degradation of 2DEG sheet resistances (R_{sh}) and mobilities (μ);[6–8] for instance, Godejohann *et al.*[7] report that, for an AlN/GaN heterostructure that was initially grown at a low temperature below 800 °C, an additional 1150 °C annealing step causes more than an 80% increase in the 2DEG R_{sh}. On the other side, GaN heterostructures with ultralow R_{sh} (<220 Ω/sq) and high μ have been realized with low-thermal budget fabrication with both MBE and MOCVD.[9–12] The mechanism behind the above correlations is intriguing. One consequence of high-temperature post-channel thermal budgets of HEMTs is interdiffusion between the epitaxial layers.[13–15] Specifically, a ternary (or quaternary) alloy would form at the interface of the barrier/GaN channel. We show here that interfacial ternary alloy formation significantly degrades 2DEG R_{sh} and μ via the ADS.

Prior to this work, Hsu and Walukiewicz[16] have established the ADS calculation for an AlGaN/GaN heterostructure with a sharp interface; Bellotti *et al.*[17] have studied how ADS impacts the μ and the drift velocity of carriers in bulk AlGaN. This work is the first analytical study of how the ADS increases with thermal budgets of GaN heterostructures. It adds technology awareness to conventional modeling of 2DEG properties.

We focus on the ADS in AlGaN/GaN heterostructures with and without an AlN IL. The ADS analysis can be generalized to other heterostructures following the procedures in Fig. 1. For simplicity, we

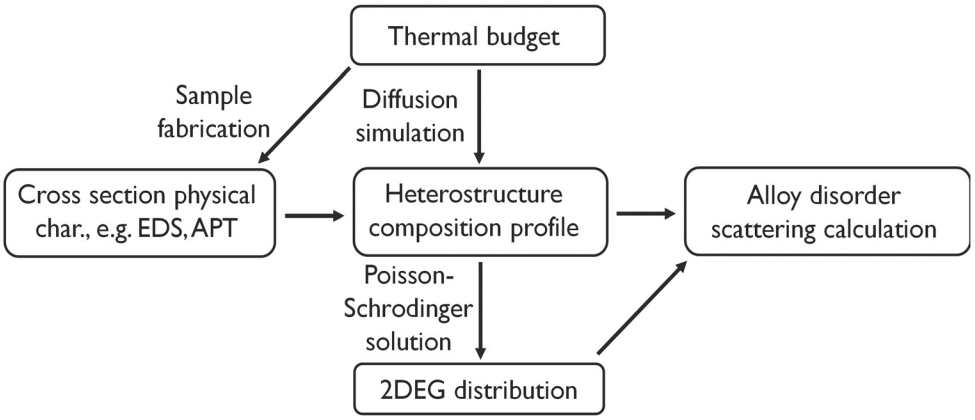

FIG. 1. Procedures to enable alloy disorder scattering calculation.

assume that interdiffusion only occurs in the direction perpendicular to the heterostructure surface (i.e., 1D approximation). The Al profile in such structures characterizes the extent of layer interdiffusion. Analogous to the calculation by Hsu and Walukiewicz,[16] the scattering rate τ_{AD} of the ADS in an AlGaN(/AlN)/GaN heterostructure is

$$\frac{1}{\tau_{AD}} = \frac{m^*\Omega U_{AD}^2}{\hbar^3}\int_{-\infty}^{\infty} \mathrm{Al}(z)(1-\mathrm{Al}(z))\left|\chi'(z)\right|^4 dz, \quad (1)$$

where m^* is the electron effective mass in the GaN conduction band, Ω is the volume of a unit cell of GaN, U_{AD} is the alloy disorder scattering potential, z is the depth perpendicular to the sample surface, Al(z) is the Al content profile in depth, and $\chi'(z)$ is the 2DEG wave function. Experimentally, the U_{AD} of $Al_xGa_{1-x}N$ can be treated as a fitting parameter, which should have a value close to the conduction band offset (~2.5 eV) or the bandgap difference (~2.8 eV) between AlN and GaN.[16,17]

To calculate τ_{AD} with Eq. (1), the composition profile and the 2DEG distribution are required. As introduced in Fig. 1, the composition profile can be derived either by layer interdiffusion simulation or by physical cross section characterizations of experimental heterostructures; accurate 2DEG distribution is essential and is derived by a 1D Poisson Schrödinger solver.[18] We will first demonstrate the ADS calculation for an exemplary 10 nm $Al_{0.25}Ga_{0.75}N$/GaN heterostructure using layer interdiffusion simulation. The thermal budget in this case arises from the 10 nm AlGaN epitaxy. Following Fick's diffusion law,

$$\frac{d\mathrm{Al}(z)}{dt} = D_{\mathrm{Al}}\frac{d^2\mathrm{Al}(z)}{dz^2}, \quad (2)$$

$$L_{D,\mathrm{Al}} = \sqrt{D_{\mathrm{Al}}t}, \quad (3)$$

where D_{Al} is the diffusion coefficient of the Al atom in $Al_xGa_{1-x}N$, t is the heating duration, and $L_{D,Al}$ is the diffusion length of the Al, which reflects the thermal budget impact. The D_{Al} and the $L_{D,Al}$ increase rapidly with temperature and have activation energies of ~2.8 and ~1.4 eV,[13] respectively. In the case of $Al_xGa_{1-x}N$/GaN stacks grown by MOCVD at >1000 °C, the $L_{D,Al}$ are usually up to 1–2 nm.[7,14,19,20] We, thus, analyze the ADS for $L_{D,Al} \leq 2$ nm in the following calculation.

Composition profiles of the 10 nm $Al_{0.25}Ga_{0.75}N$/GaN heterostructures with varied $L_{D,Al}$ are simulated in Fig. 2(a). The corresponding band diagrams, 2DEG distribution, and 2DEG centroid positions are obtained from a 1D Poisson–Schrödinger solver.[18] Several consequences of increased $L_{D,Al}$ are noted in Fig. 2: (1) overlap between the 2DEG profile and the ternary $Al_xGa_{1-x}N$ profile increases (increased 2DEG tunneling into the AlGaN barrier), (2) the 2DEG distribution stretches more in depth, and (3) the 2DEG centroid moves a small distance away from the original AlGaN/GaN interface.

As the Al(z) and the $\chi'(z)$ have been derived in Fig. 2, the scattering rate τ_{AD} as a function of the $L_{D,Al}$ can now be derived in Eq. (1). Furthermore, the ADS limited mobilities μ_{AD} are derived in Fig. 3(a) with $\mu_{AD} = \frac{q\tau_{AD}}{m^*}$, where m^* is the conduction band effective mass of GaN. The μ_{AD} is compared with the phonon limited mobility μ_{ph},[21] which is dominant in a GaN HEMT.[16,21] The μ_{ph} is derived by Gurusinghe *et al.*,[21] including deformation potential acoustic, piezoelectric acoustic, and polar optical phonon scattering mechanisms. In Fig. 3(a), the μ_{AD} decreases with the $L_{D,Al}$ and the 2DEG density N_{sh}; when the N_{sh} is large, the μ_{AD} gets comparable to the μ_{ph}. A strong impact of the ADS is, thus, expected on the R_{sh} of GaN HEMT access regions where the N_{sh} is high.

In Fig. 3(b), a lower limit of 2DEG sheet resistance $R_{sh,low}$ is calculated by considering only the phonon scattering and the ADS [ignoring other mobility degradation mechanisms like Coulomb and interface roughness scattering, see Fig. 5(c)],

$$R_{sh,low} = \frac{\mu_{ph}+\mu_{AD}}{qN_{sh}\mu_{ph}\mu_{AD}}. \quad (4)$$

The $R_{sh,low}$ in Fig. 3(b) shows how sensitive the 2DEG R_{sh} is to the ADS impact: Compared to a heterostructure with a sharp interface ($L_{D,Al}=0$), the Al diffusion into a GaN channel with $L_{D,Al}=1$ nm would cause more than 100 Ω/sq degradation of the $R_{sh,low}$. The calculation results in Fig. 3 indicate that the 2DEG μ and R_{sh} could be severely degraded by thermal budgets induced Al diffusion into the GaN channel of HEMTs.

As suggested in Fig. 1, in addition to simulation, the cross-sectional heterostructure composition profile and $L_{D,Al}$ can also be

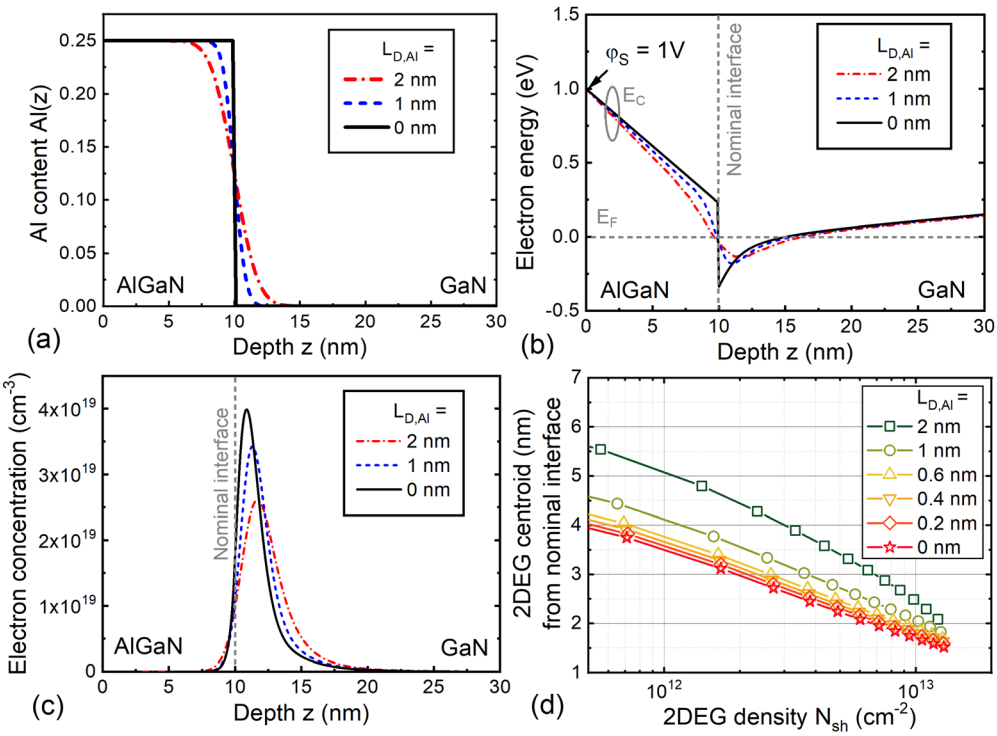

FIG. 2. Simulated (a) heterostructure composition profile, (b) band diagrams, (c) 2DEG distribution, and (d) 2DEG centroid positions of 10 nm $Al_{0.25}Ga_{0.75}N$/GaN heterostructures. Common surface potential φ_S of 1 V is assumed in (b). Common 2DEG density of 1×10^{13} cm^{-2} is assumed in (c).

read out using physical characterization methods like electron diffraction spectroscopy[7] (EDS), x-ray photoelectron spectroscopy[22] (XPS), and atom probe tomography[19] (APT). Figure 4(a) shows an EDS based Al profile from a MOCVD grown 12 nm $Al_{0.28}Ga_{0.72}N$/1 nm "AlN"/GaN sample. The MOCVD was performed at around 1000 °C; more fabrication details could be found in our previous reports.[4,23] Based on the EDS composition profile, we further calculate the 2DEG distribution [Fig. 4(a)] and μ_{AD} [Fig. 4(d)].

It is important to note how the nominal GaN heterostructure composition profile turns out experimentally after high thermal budget processing. In Fig. 4(a), an $L_{D,Al}$ of ~1 nm is noted around the AlN IL: the thermal diffusion significantly reduces the Al content of the nominal AlN IL, increases 2DEG overlapping with interfacial ternary AlGaN, increases the ADS, and eventually degrades the μ_{AD}. In addition to thermal interdiffusion, the GaN decomposition and redeposition (GDRD) effects in high-temperature epitaxy ambient[5] also

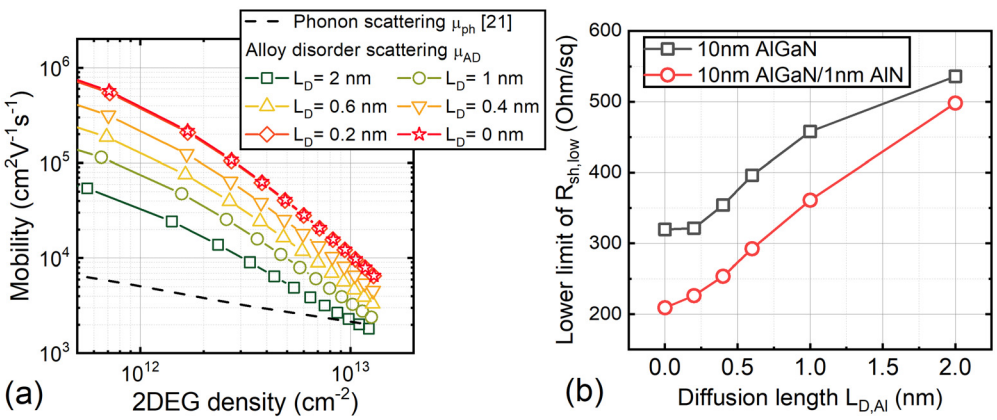

FIG. 3. Calculated ADS and phonon scattering limited (a) 2DEG mobility and (b) sheet resistance of the 10 nm $Al_{0.25}Ga_{0.75}N$/GaN heterostructure. U_{AD} = 2.5 V—the AlN/GaN conduction band offset—is assumed in calculation. $R_{sh,low}$ of 10 nm $Al_{0.25}Ga_{0.75}N$/1 nm AlN/GaN is put in (b) as comparison.

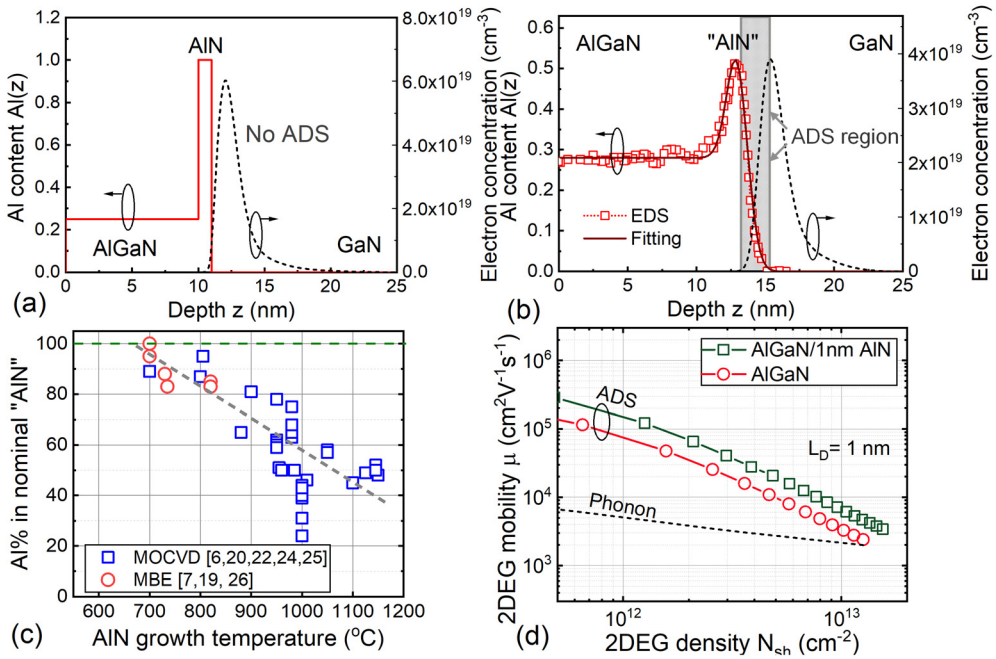

FIG. 4. Al profile (a) in nominal AlGaN/AlN/GaN and (b) in a MOCVD grown 12 nm $Al_{0.28}Ga_{0.72}N$/1 nm AlN/GaN sample. In both (a) and (b), 2DEG distribution is simulated with a total density of $1 \times 10^{13}\,cm^{-2}$. In (b), the Al profile fitting curve is simulated with $L_{D,Al} = 1$ nm; the gray zone marks the overlapping region of 2DEG and ternary $Al_xGa_{1-x}N$. (c) Literature survey of peak Al content in nominal AlN layers grown on GaN at varied growth temperature. Dropped Al% in AlN is due to Ga incorporation. The dashed lines are guides for the eye. (d) ADS limited mobility for AlGaN/GaN heterostructures with and without AlN IL, compared with the same $L_{D,Al} = 1$ nm.

worsen Al reduction (i.e., Ga incorporation) in an $Al_xGa_{1-x}N$ layer.[20,24] Note that extents of both the thermal diffusion and the GDRD increase with $Al_xGa_{1-x}N$ epitaxy temperatures. They jointly explain the observed decreasing peak Al contents in nominal AlN/GaN or barrier/AlN/GaN structures with the increase in epitaxy temperatures in numerous studies[6,7,19,20,22,24–26] [Fig. 4(b)].

In principle, a thin AlN IL in GaN heterostructures helps to improve the 2DEG mobility by pushing 2DEG wave away from the interface of the 2D well (due to a large AlN/GaN conduction band offset), thereby reducing the ADS and the interface roughness scattering of the 2DEG.[27] However, high thermal budgets induce Al content reduction in the AlN (Fig. 4) and cause ternary $Al_xGa_{1-x}N$ formation at the AlN/GaN interface; these effects increase the ADS. The negative impacts of the thermal budget on the AlN spacer effectiveness are further evidenced in literature surveys of 2DEG mobility [Fig. 5(a)] and R_{sh} [Fig. 5(b)] of GaN heterostructures.[4,11,19,20,23,26,28–39] As marked in Fig. 5(c), the scope of the surveys is limited to the N_{sh} window of 1.4×10^{13}–$1.8 \times 10^{13}\,cm^{-2}$ where the μ_{AD} impact on the total mobility μ_{tot} is significant, while the Coulomb scattering limited μ_{Coul} is insignificant. As the trends illustrated in Fig. 5(d), the μ_{Coul} and the interface roughness scattering limited μ_{IFR} would improve with increased epitaxy temperature because of decreased impurity density in and improved uniformity of epitaxial layers.[5] Therefore, the negative correlation of the μ_{tot} to thermal budgets is ascribed to the μ_{AD}.

Figures 5(a) and 5(b) suggest the universal ADS effects behind the sensitivity of 2DEG μ and R_{sh} to heterostructure processing thermal budgets. There are further experimental observations in the literature that could be explained by the ADS effects. In the studies of Mazumder *et al.*[19] and Godejohann *et al.*,[7] direct correlations are constructed between increased heterostructure thermal budgets, increased layer inter-diffusion (characterized by APT[19] and EDX,[7] respectively), reduced Al content in AlN, and degraded 2DEG μ_{tot} and/or R_{sh}; those correlations are well explained by the layer interdiffusion increased alloy disorder scattering rates.

Note several other observations in Figs. 5(a) and 5(b) that are critical for GaN HEMT technology:

(i) Estimated from the linear fitting in Fig. 5(a), lowering peak post-AlN temperature from 1050 °C to 750 °C would help to improve the mobility by significant ∼40%.

(ii) The lowest reported R_{sh} of GaN heterostructures with an AlN IL in Fig. 5(b) is very close to the minimum $R_{sh,low}$ calculated in Fig. 3(b): the best experimental R_{sh} is achieved by suppressing μ_{AD} and μ_{IFR} simultaneously while maintaining high Al content in the AlN IL to boost 2DEG density.[23,27]

(iii) While the highest μ and lowest R_{sh} are reported with molecular beam epitaxy[19] (MBE), comparable performance has been achieved by low-temperature (LT) MOCVD.[11]

(iv) The InAlN MOCVD intrinsically favors LT growth,[40] which helps to reduce the ADS compared to the usual high-temperature (HT) grown MOCVD AlGaN barrier. However, Yamada *et al.*[11] have demonstrated a LT AlGaN barrier that provides comparably low 2DEG R_{sh} to the LT InAlN.

(v) Some highest μ reported from MOCVD samples are obtained with a thin ∼1000 °C HT AlN IL and LT barrier.[4,11] As suggested in Figs. 5(c) and 5(d), the choice of the

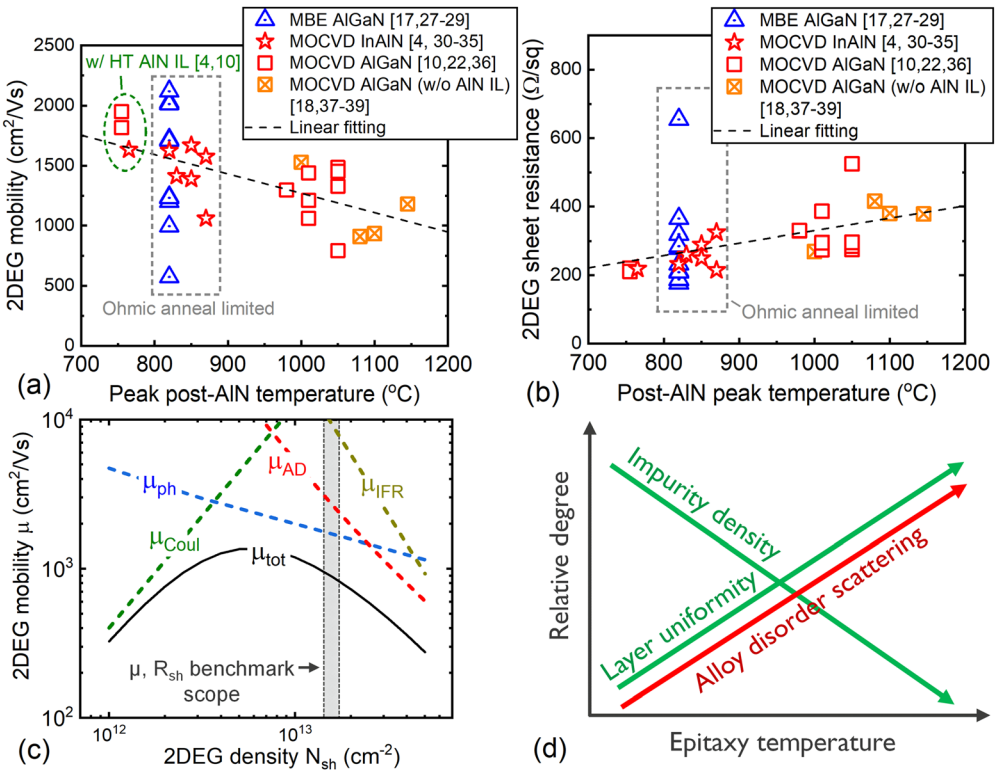

FIG. 5. Benchmarks of (a) 2DEG mobility and (b) R_{sh} of AlGaN/GaN, AlGaN/AlN/GaN, and InAlN/AlN/GaN heterostructures. The benchmark data screening criterion—N_{sh} within range of 1.4×10^{13}–1.8×10^{13} cm^{-2}—is marked in (c). Major 2DEG mobility μ_{tot} determining mechanisms, μ_{Coul}, μ_{IFR}, μ_{AD}, and μ_{ph}, are marked in (c), where dependences of μ_{Coul}, μ_{IFR}, and μ_{ph} on N_{sh} follow Refs. 16 and 21, and μ_{AD}–N_{sh} curve is from this work; exemplary μ_{tot} in (c) is calculated with Matthiessen's rule $\mu_{tot} = \left(\mu_{Ph}^{-1} + \mu_{Coul}^{-1} + \mu_{IFR}^{-1} + \mu_{AD}^{-1}\right)^{-1}$. (d) Qualitative schematic showing general trends that impurity density decreases, layer uniformity improves, but ADS worsens with the increase in epitaxy temperature.

AlN IL temperature would rely on a delicate balance between μ_{Coul}, μ_{IFR}, and μ_{AD} and, thus, requires careful experimental exploration.

(vi) The peak post-AlN temperature in several experiments[19,26,28,29,31–35] occurs in the Ohmic contact anneal step (>800 °C) instead of the barrier epitaxy step. Reducing the ADS would benefit from lowering any post-channel thermal budgets. For instance, the optimal contact anneal temperature can be lowered to <600 °C with a contact recess etch.[4,41]

With the above analysis, we reveal strong ADS impacts on the 2DEG mobility in heterostructures with high thermal budgets. As suggested by Fig. 5(c), the analytically derived thermal-budget-aware μ_{AD} contributes to accurate μ_{tot} evaluation; this would help to either predict or fit experimental 2DEG mobilities. The μ_{AD} modeling in this work would provide practical guidance for evaluating manufacturing thermal budget induced mobility degradation in GaN HEMT technology.

In summary, we construct analytical methods to calculate alloy disorder scattering (ADS) rates and the ADS limited mobility of GaN heterostructures. The simulation suggests that the ADS strongly limits the total 2DEG mobility. Because the ADS increases with intermixing between the GaN channel and the barrier materials, the post-channel thermal budget of GaN HEMTs directly degrades the 2DEG mobility via the ADS mechanism. The theoretical prediction of the adverse thermal budget and ADS impacts on the 2DEG mobility aligns with universal literature observations. The findings suggest that careful balance of the optimal temperature window and the thermal budget of processing steps is critical to optimizing GaN technology.

AUTHOR DECLARATIONS

Conflict of Interest

The authors have no conflicts to disclose.

DATA AVAILABILITY

The data that support the findings of this study are available within the article.

REFERENCES

[1]U. K. Mishra, L. Shen, T. E. Kazior, and Y. F. Wu, Proc. IEEE **96**, 287 (2008).
[2]M. Micovic, D. F. Brown, D. Regan, J. Wong, Y. Tang, F. Herrault, D. Santos, S. D. Burnham, J. Tai, E. Prophet, I. Khalaf, C. McGuire, H. Bracamontes, H. Fung, A. K. Kurdoghlian, and A. Schmitz, in *IEEE International Electron Devices Meeting* (IEEE, 2016), pp. 59–62.
[3]N. Collaert, A. Alian, A. Banerjee, V. Chauhan, R. Y. ElKashlan, B. Hsu, M. Ingels, A. Khaled, K. V. Kodandarama, B. Kunert, Y. Mols, U. Peralagu, V. Putcha, R. Rodriguez, A. Sibaja-Hernandez, E. Simoen, A. Vais, A. Walke, L. Witters, S. Yadav, H. Yu, M. Zhao, P. Wambacq, B. Parvais, and N. Waldron,

in *ECS Meeting Abstracts MA2020-02, 1707* (The Electrochemical Society, 2020).
[4]U. Peralagu, B. de Jaeger, D. M. Fleetwood, P. Wambacq, M. Zhao, B. Parvais, N. Waldron, N. Collaert, A. Alian, V. Putcha, A. Khaled, R. Rodriguez, A. Sibaja-Hernandez, S. Chang, E. Simoen, S. E. Zhao, B. de Jaeger, D. M. Fleetwood, P. Wambacq, M. Zhao, B. Parvais, N. Waldron, and N. Collaert, in *IEEE International Electron Devices Meeting* (IEEE, 2019), pp. 398–401.
[5]D. D. Koleske, A. E. Wickenden, R. L. Henry, W. J. DeSisto, and R. J. Gorman, J. Appl. Phys. **84**, 1998 (1998).
[6]X. X. Zheng, C. H. Lin, D. Ueda, and E. Y. Chang, Thin Solid Films **709**, 138228 (2020).
[7]B. J. Godejohann, E. Ture, S. Müller, M. Prescher, L. Kirste, R. Aidam, V. Polyakov, P. Brückner, S. Breuer, K. Köhler, R. Quay, and O. Ambacher, Phys. Status Solidi B **254**, 1600715 (2017).
[8]C. Pan, C. Li, Z. Li, D. Peng, D. Zhang, Q. Yang, Y. Sun, and S. Wu, J. Cryst. Growth **531**, 125265 (2020).
[9]Y. Cao and D. Jena, Appl. Phys. Lett. **90**, 182112 (2007).
[10]Y. Cao, K. Wang, G. Li, T. Kosel, H. Xing, and D. Jena, J. Cryst. Growth **323**, 529 (2011).
[11]A. Yamada, J. Yaita, N. Nakamura, and J. Kotani, J. Cryst. Growth **560–561**, 126046 (2021).
[12]J. Xue, J. Zhang, and Y. Hao, Appl. Phys. Lett. **107**, 043503 (2015).
[13]I. A. Aleksandrov, T. V. Malin, K. S. Zhuravlev, S. V. Trubina, S. B. Erenburg, B. Pecz, and Y. V. Lebiadok, Appl. Surf. Sci. **515**, 146001 (2020).
[14]D. Cai, X. Chen, H. Xu, N. Lin, F. Xu, and H. Chen, Jpn. J. Appl. Phys. **52**, 100207 (2013).
[15]N. Chaaben, J. Laifi, H. Bouazizi, C. Saidi, A. Bchetnia, and B. El Jani, Mater. Sci. Semicond. Process. **42**, 359 (2016).
[16]L. Hsu and W. Walukiewicz, Phys. Rev. B **56**, 1520 (1997).
[17]E. Bellotti, F. Bertazzi, and M. Goano, J. Appl. Phys. **101**, 123706 (2007).
[18]G. L. Snider, I. H. Tan, and E. L. Hu, J. Appl. Phys. **68**, 2849 (1990).
[19]B. Mazumder, S. W. Kaun, J. Lu, S. Keller, U. K. Mishra, and J. S. Speck, Appl. Phys. Lett. **102**, 111603 (2013).
[20]H. Li, S. Keller, S. H. Chan, J. Lu, S. P. Denbaars, and U. K. Mishra, Semicond. Sci. Technol. **30**, 055015 (2015).
[21]M. N. Gurusinghe, S. K. Davidsson, and T. G. Andersson, Phys. Rev. B **72**, 045316 (2005).
[22]A. Yamada, T. Ishiguro, J. Kotani, S. Tomabechi, and N. Nakamura, Phys. Status Solidi B **254**, 1600496 (2017).
[23]H. Yu, A. Alian, U. Peralagu, M. Zhao, N. Waldron, B. Parvais, and N. Collaert, IEEE Trans. Electron Devices **68**(11), 5559 (2021).
[24]S. Dai, H. Gao, Y. Zhou, Y. Zhong, J. Wang, J. He, R. Zhou, M. Feng, Q. Sun, and H. Yang, J. Phys. D: Appl. Phys. **51**, 035102 (2018).
[25]A. Yamada, T. Ishiguro, J. Kotani, and N. Nakamura, Jpn. J. Appl. Phys. **57**, 01AD01 (2018).
[26]S. W. Kaun, B. Mazumder, M. N. Fireman, E. C. H. Kyle, U. K. Mishra, and J. S. Speck, Semicond. Sci. Technol. **30**, 055010 (2015).
[27]L. Shen, S. Heikman, B. Moran, R. Coffie, N. Q. Zhang, D. Buttari, I. P. Smorchkova, S. Keller, S. P. DenBaars, and U. K. Mishra, IEEE Electron Device Lett. **22**, 457 (2001).
[28]S. W. Kaun, M. H. Wong, U. K. Mishra, and J. S. Speck, Appl. Phys. Lett. **100**, 262102 (2012).
[29]S. W. Kaun, P. G. Burke, M. Hoi Wong, E. C. H. Kyle, U. K. Mishra, and J. S. Speck, Appl. Phys. Lett. **101**, 262102 (2012).
[30]S. Guo, X. Gao, D. Gorka, J. W. Chung, H. Wang, T. Palacios, A. Crespo, J. K. Gillespie, K. Chabak, M. Trejo, V. Miller, M. Bellot, G. Via, M. Kossler, H. Smith, and D. Tomich, Phys. Stat. Solidi A **207**, 1348 (2010).
[31]J. W. Chung, O. I. Saadat, J. M. Tirado, X. Gao, S. Guo, and T. Palacios, IEEE Electron Device Lett. **30**, 904 (2009).
[32]D. S. Lee, J. W. Chung, H. Wang, X. Gao, S. Guo, P. Fay, and T. Palacios, IEEE Electron Device Lett. **32**, 755 (2011).
[33]H. S. Lee, D. Piedra, M. Sun, X. Gao, S. Guo, and T. Palacios, IEEE Electron Device Lett. **33**, 982 (2012).
[34]D. S. Lee, X. Gao, S. Guo, and T. Palacios, IEEE Electron Device Lett. **32**, 617 (2011).
[35]D. S. Lee, X. Gao, S. Guo, D. Kopp, P. Fay, and T. Palacios, IEEE Electron Device Lett. **32**, 1525 (2011).
[36]C. Wang, X. Wang, G. Hu, J. Wang, H. Xiao, and J. Li, J. Cryst. Growth **289**, 415 (2006).
[37]S. Arulkumaran, T. Egawa, H. Ishikawa, and T. Jimbo, J. Vac. Sci. Technol. B **21**, 888 (2003).
[38]G. Ding, L. Guo, Z. Xing, Y. Chen, P. Xu, H. Jia, J. Zhou, and H. Chen, Sci. China Phys. Mech. Astron. **53**, 49 (2010).
[39]M. Miyoshi, M. Sakai, H. Ishikawa, T. Egawa, T. Jimbo, M. Tanaka, and O. Oda, J. Cryst. Growth **272**, 293–299 (2004).
[40]M. Gonschorek, J. F. Carlin, E. Feltin, M. A. Py, and N. Grandjean, Appl. Phys. Lett. **89**, 062106 (2006).
[41]A. Firrincieli, B. de Jaeger, S. You, D. Wellekens, M. van Hove, and S. Decoutere, Jpn. J. Appl. Phys. **53**, 04EF01 (2014).